AVIATION

THE INTERPLAY BETWEEN GEOMETRY AND NUMBERS OF BLADE IN DUCTED PROPELLER SYSTEMS

Muhammad DZULFIKAR [1✉], Helmy PURWANTO [1], Muhammad Abdul WAHID [1],
Prima Adhi YUDHISTIRA [2]

[1]*Department of Mechanical Engineering, Faculty of Engineering, Universitas Wahid Hasyim, Semarang, Indonesia*
[2]*Department of Mechanical Engineering, Faculty of Engineering, Diponegoro University, Semarang, Indonesia*

Abstract. This study designs and optimizes a ducted propeller (DP) via graphical and numerical methods. Ducted propellers with a thrust-to-omega ratio ranging between 0.12 and 0.20 and blade optimizations at the design point were obtained. The geometric selection of the blade path has a significant effect on the airflow in the duct system. Reasonable optimization of the dimensions of the sheath, tube, and curvature can effectively improve the axial flow. For different aerodynamic loads, the corresponding graphs are produced. Therefore, the number of blades increases, and the overall stall margin is expanded for a particular blade. The large discrepancy between the mechatronic properties of experimental and computational studies of DPs implies that the blade geometry can largely affect the mechatronic properties of DP models, thus offering a new direction for designing the development of propulsion systems. In this article, important studies on the impact of the blade geometry and number on DP thrust generation are discussed.

Notations

Variables and functions

S_2 – area of the propeller disc;
S_F – area at the actuator disc;
T – total thrust;
T_D – ducted thrust;
T_{DP} – ducted propeller thrust;
V_1 – velocity at the actuator disc;
V_4 – far wake velocity;
Δp – static pressure rise;
ρ – air density;
σ – duct diffusion ratio.

Abbreviations

AM – additive manufacturing;
CAD – computer aided design;
CFD – computational fluid dynamics;
DP – ducted propeller;
FEM – finite element method;
NACA – National Advisory Committee for Aeronautics.

1. Introduction

Consistent efforts to find efficient propulsion systems are resulting in major changes in the aeromodeling ecosystem. Ducted propellers, commonly called electric ducted fans, are popular propulsion systems in the aeromodeling world and are usually applied to relatively small aerial vehicles or drones (Nugroho et al., 2018; Sharman, 2011; Toguchi et al., 2016; Zhang & Barakos, 2020).

Thrust generation from electric propulsion systems has become a topic of interest for addressing the need for exploration and transportation (Moeckel, 1963; Weintraub et al., 2022). Using computational fluid dynamics (CFD) as a simulation tool provides a way to achieve faster production of high-technology products at relatively lower costs than conventional trial–error processes do (Akturk & Camci, 2012; Karpuk et al., 2022; Versteeg & Malalasekera, 2007). However, the generation of thrust and energy propulsion is challenging because a ducted propeller is an extremely complicated system due to its many elements (Drela & Youngren, 2005; Harada, 2018; Seitz, 2012). Therefore, a meticulous process is needed to engineer DPs into more effective products and systems.
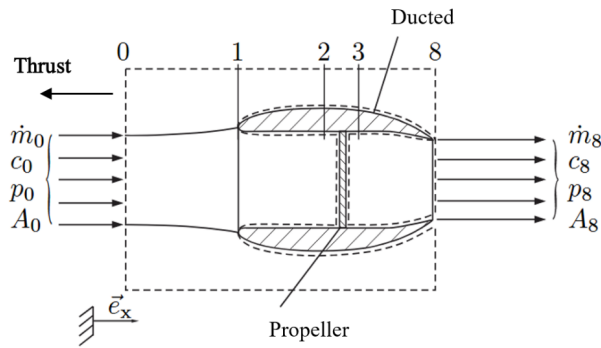
Figure 1. The airflow passes through the channeled propulsion system (source: Weintraub, 2024)

Comprehensive studies have been reported regarding the design of DPs for generating thrusts (Geldenhuys, 2015; Urban et al., 2023; Zhang, 2022). Recently, significant progress has been made in the design of DP systems with higher energy and velocity impacts. Several design and manufacturing methods, such as CAD, FEM, CFD, and AM, have been successfully integrated to construct systems (Ganesan et al., 2022; Iljaszewicz et al., 2020; van Rooij, 2019). Moreover, the number of articles related to these topics has significantly increased to follow the frontier of the electric and digital technology era. Several software and CAD applications, e.g., Catia, Ansys, Abaqus, and Solidworks, can be utilized to build the DP into a more powerful system (SolidWorks, n.d.).

Brusell et al. (2017) and Dzulfikar et al. (2022) conducted tests to evaluate the thrust force of electric ducted fans via experimental methods. Experimental testing (Stosiak et al., 2018) is carried out to determine the flow of liquid through a pipe system via experimentation, analysis, and the finite volume element method of numerical modeling. Jiang et al. (2022) conducted experiments and simulation tests via Ansys CFX with the addition of outlets to deepen and recognize undected and ducted propeller characteristics. The literature (Fan et al., 2020; Goudswaard, 2021; Muehlebach & D'Andrea, 2017; Zhang, 2022) provides an understanding of DP configurations and their aerodynamic performance. However, this paper focused on the interplay between the geometry and number of blades in the DP

system from a simulation overview. Owing to SolidWorks, easy-to-use and broad tools for supporting solid and fluid modeling exist. Notably, the role of airfoil selection and the number of blades and their relationship with their thrust generation in the DP system are discussed.

This study aims to describe the impact and interplay between various airfoil geometries and blade quantities of ducted propeller systems on thrust generation. A simulation method incorporating rotational speed variation was selected, followed by validation of the results through experimental data and numeric-analytical findings from other studies. The thrust-generating features and fluid flow properties are studied in depth, with a special emphasis on the geometry interplay. The thrust generating system from ducted propeller shown in Figure 1.

2. Ducted propeller performance identification method

2.1. Geometry and number of blade models

The propeller design stage is carried out first before the simulation process.

The modelling flowchart is schematically shown in Figure 2. The various blade profiles used are the Bergey BW series and the NACA 7 series. The blade designs with various profiles are shown in Figure 3, which shows the Bergey blade, the NACA blade, and the DP system.
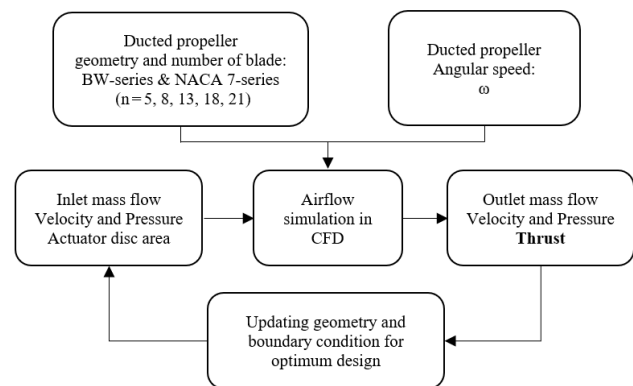

Figure 2. Modeling flowchart (source: created by authors)
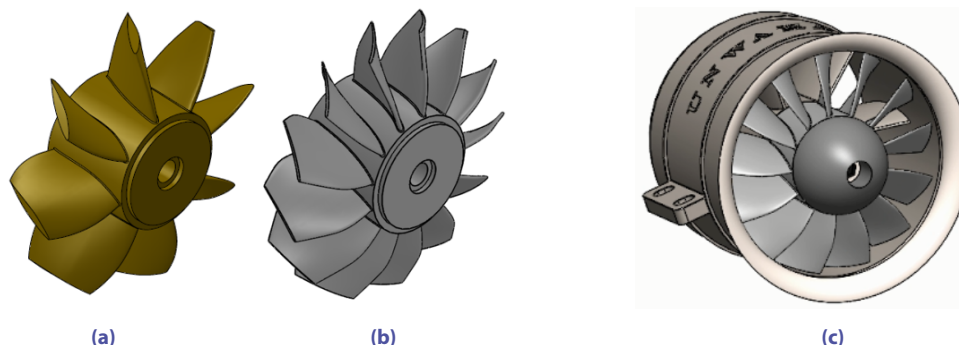

(a)   (b)   (c)

Figure 3. Variation in the geometry and number of blades: (a) – NACA 7 series with 8 blades; (b) – Bergey BW series with 13 blades; and (c) – the ducted propeller system (source: created by authors)

The NACA 7-series airfoil section has a greater probability of laminar flow at the lower surface than at the upper surface (Hassen, 2021; Liu, 2021; Panigrahi & Mishra, 2014). This section provides a low throw moment coefficient while maintaining a suitably high design lift coefficient at the cost of some reduction in the maximum lift and critical Mach number. This blade has a thickness ratio of 15% (Abbott & Doenhoff, 1959).

The Bergey BW series is known for the cambered thin airfoil with 5% t/c (Giguère & Selig, 1997; Pope, 1951; Selig, 2003).
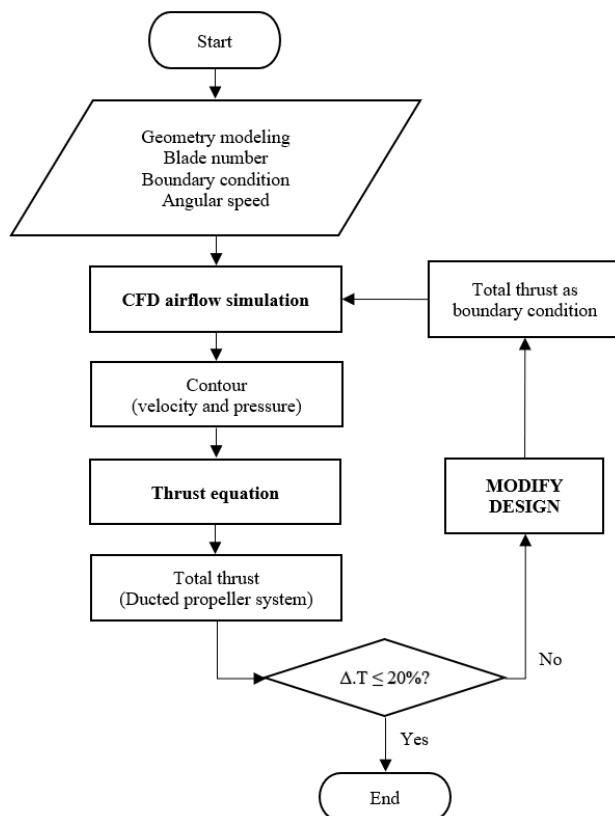

Figure 4. Simulation procedure (source: created by authors)

2.2. Computational fluid dynamic simulation

Computational fluid dynamics is a method that employs computational technology or computer-based simulation to analyze airflow circulation phenomena (Versteeg & Malalasekera, 2007). Computational fluid dynamics (CFD) is a subfield of fluid mechanics that employs numerical methods and algorithms to solve problems and identify solutions in both industrial and nonindustrial applications, such as rotorcraft aerodynamics (Zhang et al., 2022). The three approaches that can be employed to address engineering problems are analytical, experimental, and numerical simulations (Schäfer, 2006; Stosiak et al., 2018).

After completion of the blade design process, the next step involves the assembly of the blade with other DP components to form a complete DP. The simulation method is conducted via SOLIDWORKS 2021 software, specifically for external flow simulation. This repeated method provides a dataset on axial flow, pressure, and thrust.

This research involves modifying the propeller by adjusting the geometry and number of blades, which is then executed with SolidWorks simulations of fluid dynamics to determine thrust generation. Then, a wind tunnel model is developed for setting the boundary conditions. With dimensions of 200 × 200 mm, the samples were extruded to 600 mm with a thickness of 2 mm, the inlet and outlet sides were covered with extruded boss 2 mm thick, and the merge result feature was turned off. The final outcome is depicted in Figure 4. The next step is to assemble the duct housing, propeller, front cone, and wind tunnel so that it looks like in Figure 5.

In this study, several stages of the simulation process were carried out:
1. Preprocessing
a. Domain Computing (Field)

In the computational field, a solid area (ducted prop.) and a fluid area (air). Figure 4 illustrates the 3-dimensional space geometry in which the computational field is conditioned as a wind tunnel replacement simulation model.
b. Meshing (Field Arrangement)

After the ducted propeller (DP) geometry is drawn and the computational domain is formed, the next process is
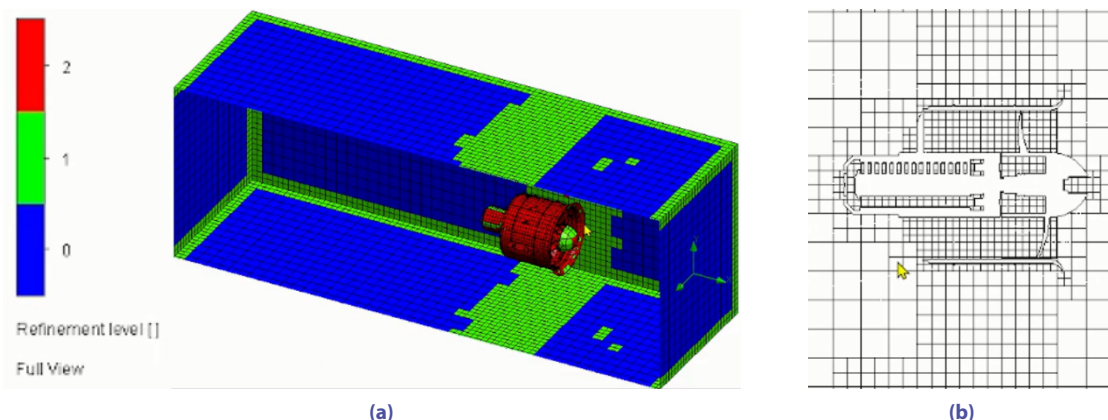

Figure 5. Meshing system: (a) – global mesh and (b) – cut plot 2D mesh (source: created by authors)

186

M. Dzulfikar et al. The interplay between geometry and numbers of blade in ducted propeller systems

meshing, which can be seen in Figure 5 via SolidWorks meshing software. The blue color indicates a refinement level of 0, which corresponds to the largest rectangular area. In the green color, refinement level 1 has a more detailed meshing of four squares from level 0. The greatest detail of the meshing area is shown in red. It has approximately 16 squares compared with level 0.

c. Boundary condition

After meshing, the boundary conditions are set as follows: inlet (front DP), outlet (rear DP), symmetry 1 (top and bottom of the DP), and symmetry 2 (right and left DP).

2. Processing

At this stage, several parameters are set according to the simulation needs, namely, the fluid airflow around the prop that is channeled, as shown in Table 1.

Table 1. Simulation parameters

Parameter Simulation	Value
Unit System	80 mm Inner diameter
Angular velocity	50k Rotation per minutes
Analysis type	Internal
Physical features	Rotational
Fluids	Air with density of 1.225 kg/m3
Flow characteristics	Laminar & turbulent
wall conditions -Roughness	0 micrometer
Pressure	101325 Pascal

3. Postprocessing

a. Numerical data

The simulation is performed by changing the fluid flow to the other variants, and the data that can be taken are V_x, P, and F_T. The parameter unit system of the ducted propeller used in this study is shown in Table 2.

Table 2. Simulation object

Parameter Unit System	Airfoil	
	NACA 7 series	Bergey BW
Duct Inner Diameter (mm)	81	
Tip Diameter (mm)	80	
Hub Diameter (mm)	35	
Number of Blades	5, 8, 13, 18, 21	
Rotational Speeds (rpm)	40000, 45000, 50000	

b. Picture data

In addition to obtaining numerical data, we can also obtain image or contour data with color gradations obtained in the postprocessing step.

3. Numerical analysis

The experiments were implemented within the SolidWorks environment. For each variation, the DP simulations were conducted twice. Entering the same parameters ensures that the geometry and other data remain unchanged.

Hence, the following data are collected. Table 3 below shows that the data can be converted into a curve, as shown in Figure 6.

Table 3. Selective results

Propeller Type	T (N)	ω (rpm)	ratio T: ω in rad/s
B-13	26.9	50000	0.20
B-5	23	50000	0.17
B-5	19.4	45000	0.16
N-21	15.9	45000	0.13
N-8	16.7	40000	0.16
N-21	12.6	40000	0.12

3.1. Effect of the number of blades and propeller airfoil geometry

The curve in Figure 6 illustrates that the thrust force generated by the DP from each variant of the propeller type continues to rise as the rotation of the DP electric motor (rotations per minute) increases. The thrust force of the N-21 ducted propeller with a 40000 rpm variation was 12.6 N, which increased by 26% to 15.9 N at 45000 rpm. The thrust force in the B-5 system was 19.4 N at 45000 rpm and increased by 19% to 23 N at 50000 rpm. The thrust-to-angular velocity ratio subsequently varied between 0.12 and 0.20.

In Figure 6, the NACA and Bergey ducted propellers that were tested are illustrated. The NACA DP achieves its optimal performance in the 8-blade variant, where the thrust values increase from 16.7 N to 22.6 N for a 20% increase in motor speed (40,000 rpm vs. 50,000 rpm). Moreover, the best Bergey blade variant was achieved with a total of 13 blades. Motor rotation at 40k rpm and 50k rpm resulted in an increase in thrust from 21.7 N to 26.9 N.

Conversely, the Bergey airfoil was the optimal setting geometry for the maximum angular velocity angle of view in the case of an 8-blade propeller. Nevertheless, the NACA 7 series is equipped with a sturdier blade that is capable of operating within the 80% angular velocity range of the motor drive.
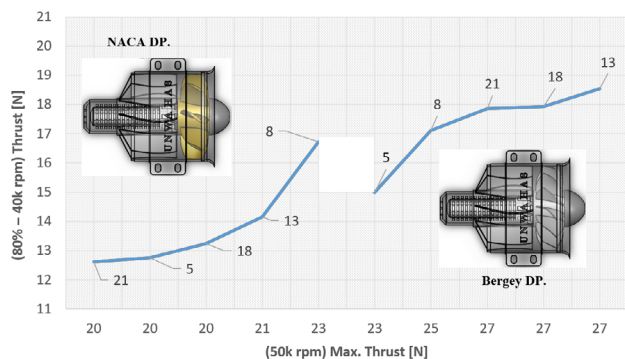

Figure 6. The effect of the interplay between the geometry and number of blades on the thrust generated by a ducted propeller system (source: created by authors)

3.2. The effect of interactions on airflow simulation

The fluid flow phenomenon through the ducted propeller was determined through a SolidWorks simulation. Two varieties of blades were chosen to show the fundamental differences between the samples: NACA series 7, with a thickness ratio of 15%, and Bergey, with a thickness ratio of 5%.

Different thrusts were measured during the motor's rotation at 40000 and 50000 rpm. To understand the impact of the rotational speed and the interaction of various blade geometries and numbers on the aerodynamic performance, the angular velocity was considered a variable. The flow patterns of types B-13, with a speed of 50k rpm, and N-21, with a speed of 40k rpm, exhibit the greatest disparity in thrust values. The flow simulation in Solid-Works was employed to generate the thrust force. The sample datasheet was created by compiling the derived flow trajectories, pressures, and velocities and subsequently conducting feature extraction.

Figure 7 sequentially shows the distribution of airflow around the DP with a variation in the number of Bergey 13 blades. The air density through B-13 results in a tapered and dense flow shape. The thin blade character of Bergey, with its curvature, allows the wind to pass easily at high speed. The wind speed at the outermost side of the blades, as it passes through the shrouded fan, ranges between 49.7 and 80.6 m/s.

Figure 8 sequentially shows the distribution of airflow around the DP with variations in the NACA 21 blades. The sweep area of the N-21 fan, which is arranged with 21 blades, looks very tight. The 15% thickness ratio of the NACA 7 series blades creates a stretching phenomenon in the airflow. The shape of the flow when exiting the ducted propeller is similar to a hollow vortex with a wide diameter. The wind speed at the tip of the inner blade is 33–61 m/s.

Figures 9 and 10 show the pressure contour plot at the surface of the ducted propeller in the cut plot region. The findings reveal the various phenomena associated with flow simulation. The color in Figure 9 is characterized by a bluish–green hue and can be interpreted as the pressure distribution at the wind entry face, which is between 95 and 100 kPa. Then, the pressure increases to approximately 100–105 kPa at the blade tip region inside the sheath.

In Figure 10, 13 Bergey-type blades rotate at a speed of 50 krpm. The result is pressure variation in the area of the ducted propeller face and the inner blade tip. The pressure increased from light blue (91 kPa) to bright yellow (108 kPa). The predominance of bright colors indicates high compression pressure through the ducted propeller blades. This shows the effectiveness of the thin and concave blades in sucking in the wind.
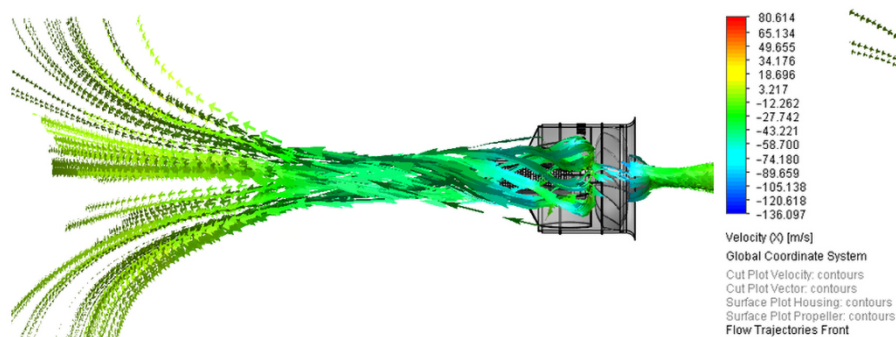

Figure 7. Airflow on B-13 was conducted at 50000 rpm (source: created by authors)
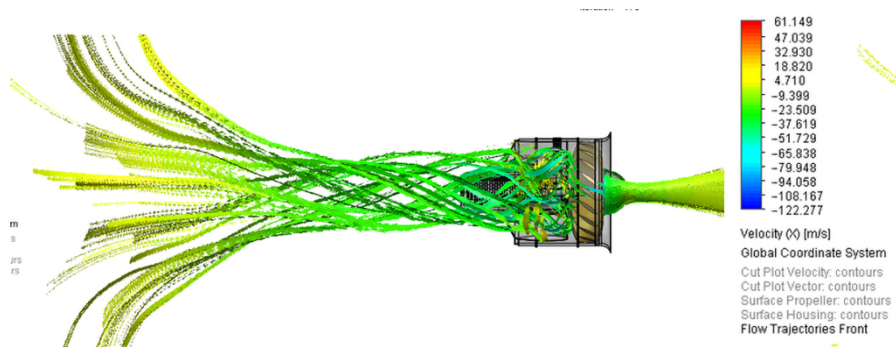

Figure 8. Airflow on the N-21 duct Prop at 40000 rpm (source: created by authors)
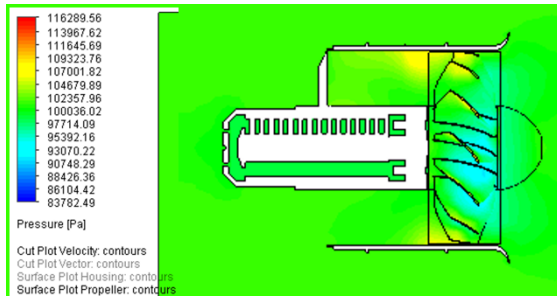
Figure 9. Pressure gradient in N-21 channel buffer at 40000 rpm (source: created by authors)
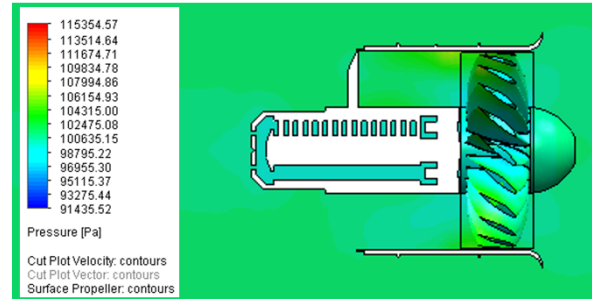

Figure 10. Pressure gradient at the B-13 duct support at a speed of 50000 rpm (source: created by authors)

4. Discussion

There has been substantial progress in the development of mathematical simulation technology and computational fluid dynamics. Anderson and Bowden (2022) presented a new theory of flight. Researchers have discovered that the actual flow (turbulent) can be computed and understood following the Kutta condition, potential flow, elegance, and 3D rotational slip separation.

Then, Voogd (2020) proposed a new experimental investigation method for the ingestion of boundary layers in integrated propulsion systems. This method identified a relatively new definition of propelling efficacy. Fan et al. (2020) conducted a parametric analysis of a ducted fan rotor via a free-form method. They discovered that the efficiency and pressure ratio are enhanced by the blade twist and sweep through computation. Harada et al. developed a ducted fan optimal design program, OptDuct (Masashi, 2022). They calculated the configuration of the "ducted propeller" with the highest efficiency.

In this work, the emphasis is on the interaction between the geometry and number of blades in the ducted propeller aerodynamic performance. Geometry and number of blades associated with the aerodynamic performance of the ducted propeller. The CFD analysis and static test bench results revealed that the propeller's angular speed can be engineered to be 50% of the real constraint. More studies were implemented with blade specifications from the NACA 65 series (Kriebel & Mendenhall, 1964; Ryu et al., 2017; van Rooij, 2019).

Bergey airfoils are thin and curved blades. Airflows faster at the curved part of the blade and rotates faster to increase its energy.

The optimization results of the propeller suggested that the airfoil Bergey of the blade increased gradually as the number of blades increased. This result was dissimilar from that of the NACA blade; from the CFD simulation, a blade number of 8 had the best performance at every angular speed. The addition of blade number for the NACA airfoil decreases the resultant thrust from 10% to 25% lower than the optimum design, as shown in Figure 6.

From a numerical point of view, the ratio of thrust to omega varies from 0.12 to 0.20 for different geometries, and the number of blades for similar angular velocities is displayed in Table 3.

An early study (Jiang et al., 2022; Masashi, 2022; Weintraub et al., 2022) that evaluated a duct fan lifting system revealed that the aerodynamic effect of the duct on the fan was quantified via momentum theory. Equations (1) from the Jiang model and (2) from the Masashi model, as shown in Figure 11, were used to calculate and validate the thrust of the ducted propeller.

$$T_{DP} = S_2\left(\Delta p\right) + T_D = \rho\sigma S_2 V_4^2; \qquad (1)$$

$$T = \rho S_F V_1^2, \qquad (2)$$

where ρ is the air density, S_F and S_2 are the areas of the propeller disc, σ is the duct diffusion ratio, V_1 is the velocity at the actuator disc and V_4 is the far-wake velocity.

The ducted propeller thrust obtained from numerical analysis was validated via experimental data generated from (Dzulfikar et al., 2022). Interplay between the geometry and number of blades, indicating three samples: the FMS airfoil model with 12 blades, the NACA 7 series with 8 blades, and the Bergey model with 13 blades. For the 40000 rotational speed of the blades, the numerical results agreed well with the experimental results according to the present model. The more the propeller rotates, the greater the thrust force produced. At the experimental side, it becomes steeper than from the numerical point of view, as shown in Figure 12.

The aforementioned results confirmed the extensive potential of SolidWorks flow simulation. After the data and knowledge obtained in the ducted propeller geometry optimization study in this paper, several challenges need to be evaluated and investigated. These challenges include
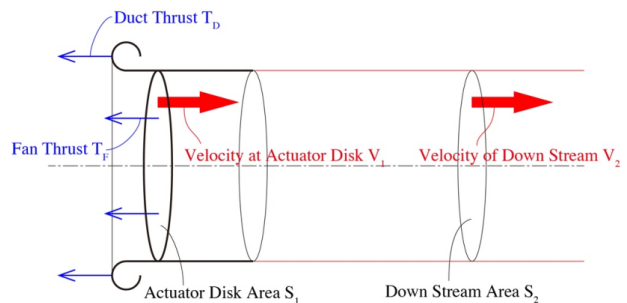

Figure 11. Ducted propeller system free body diagram (source: Masashi, 2022)
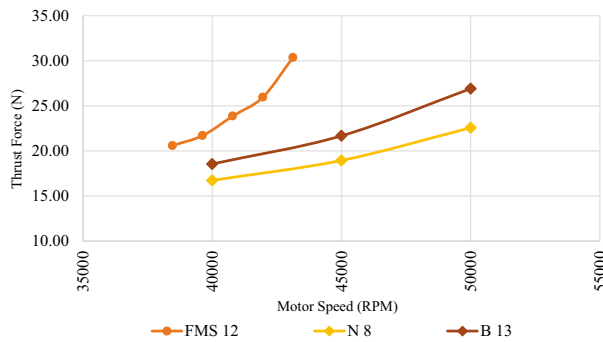
Figure 12. Comparison and validation of the thrust generated by the Ducted Propeller from numerical simulations (N 8 and B 13) and the experimental setup (FMS 12)

the comprehensive scope of parametric systems, various numerical simulations and mathematical backgrounds, material and vibration mechanics, and the application of ducted propellers on rotorcraft or UAVs (Zhang et al., 2022; Zhang & Barakos, 2020).

5. Conclusions

In this SolidWorks simulation, the aerodynamic performance of the ducted propeller system was clarified. The interplay between geometry and numbers of blade in ducted propeller system has been investigated. Two types of blades were evaluated: Bergey BW series and NACA 7 series. Blade geometry was found to be impactful for the ducted propeller systems at certain number of blade. The Bergey DP has a higher thrust generation than that for NACA DP systems. This is because the airflow from Bergey DP is better than that of NACA DP systems. Therefore, a model of proper ducted propeller systems is needed to generating thrust. The model has been simulated on the SolidWorks and results show that the DP systems simulates the change of the thrust generation quite accurately. The real actuator disk area between the hub and the duct is a key factor that impacts the interplay between geometry and numbers of blade in ducted propeller systems.

The final conclusion is that a great deal of research on modelling and simulation of ducted propeller systems have been made, but there is still a need for further research. A future research objective is to study the dynamic interaction between ducted propeller parts and the total propulsion system of aircraft in detail.

Acknowledgements

Author contributions

MD conceived the study and was responsible for the design and extraction of the data. MAW and PAY were responsible for data interpretation and reviewed the article; HP supervised the article; PAY conceived the idea; MD, MAW and HP obtained the funding and were responsible for analysis; and MD wrote and revised the article.

Disclosure statement

Authors declare not to have any competing financial, professional, or personal interests from other parties.

References

Abbott, I. H., & Doenhoff, A. E. Von. (1959). *Theory of wing sections: Including a summary of airfoil data*. Dover Publications, Inc.

Akturk, A., & Camci, C. (2012). Experimental and computational assessment of a ducted-fan rotor flow model. *Journal of Aircraft*, *49*(3), 885–897. https://doi.org/10.2514/1.C031562

Anderson, J. D., & Bowden, M. L. (2022). *Introduction to flight* (9th ed.). McGraw-Hill Education.

Brusell, A., Andrikopoulos, G., & Nikolakopoulos, G. (2017). Novel considerations on the negative pressure adhesion of electric ducted fans: An experimental study. In *25th Mediterranean Conference on Control and Automation* (*MED*) (pp. 1404–1409). ResearchGate. https://doi.org/10.1109/MED.2017.7984315

Drela, M., & Youngren, H. (2005). Axisymmetric analysis and design of ducted rotors. In *Theory Document of DFDC* (pp. 1–20). https://web.mit.edu/drela/Public/web/dfdc/DFDCtheory12-31.pdf

Dzulfikar, M., Priangkoso, T., Setiawan, J. D., & Sportyawan, C. W. (2022). Analisis Propulsi Statik dari Electric Ducted Fan dengan Metode Eksperimental [Static propulsion analysis of electric ducted fan using experimental method]. *Jurnal Ilmiah Momentum*, *18*(2), 124–127. https://doi.org/10.36499/jim.v18i2.7281

Fan, C., Adjei, R. A., & Wang, A. (2020). Parametric study on the aerodynamic performance of a ducted-fan rotor using free-form method. *Aerospace Science and Technology*, *101*, Article 105842. https://doi.org/10.1016/j.ast.2020.105842

Ganesan, S., Esakki, B., Mathiyazhagan, S., & Pandimuthu, V. (2022). Design conception and evaluation of an unmanned amphibious aerial vehicle using systematic approach. *Aviation*, *26*(1), 41–53. https://doi.org/10.3846/aviation.2022.16519

Geldenhuys, H. J. (2015). *Aerodynamic development of a contra-rotating shrouded rotor system for a UAV*. Stellenbosch University. http://hdl.handle.net/10019.1/97056

Giguère, P., & Selig, M. S. (1997). Low Reynolds number airfoils for small horizontal axis wind turbines. *Wind Engineering*, *21*(6), 367–380.

Goudswaard, R. (2021). *Aerodynamic performance of a small-scale ducted rotor in hover* [Master Thesis, Delft University of Technology]. TU Delft.

Harada, M. (2018). Design of maximum thrust ducted fan. *Journal of the Japan Society for Aeronautical and Space Sciences*, *66*(3), 75–83. https://doi.org/10.2322/jjsass.66.75

Hassen, A. E. (2021). Flow characterization in mine ventilation fan blade design using CFD. *Journal of Sustainable Mining*, *20*(3), 144–156. https://doi.org/10.46873/2300-3960.1063

Iljaszewicz, P., Łusiak, T., Pastuszak, A., & Novak, A. (2020). Aerodynamic analysis of the aircraft model made with the 3D printing method. *Transportation Research Procedia*, *51*, 118–133. https://doi.org/10.1016/j.trpro.2020.11.014

Jiang, H., Zhou, Y., & Ho, H. W. (2022). Aerodynamic design and evaluation of a ducted fan lift system for vertical takeoff and landing flying cars. *Proceedings of the Institution of Mechanical Engineers, Part A: Journal of Power and Energy*, *237*(1), 115–125. https://doi.org/10.1177/09576509221106395

Karpuk, S., Radespiel, R., & Elham, A. (2022). Assessment of future airframe and propulsion technologies on sustainability of next-generation mid-range aircraft. *Aerospace*, *9*(5), Article 279. https://doi.org/10.3390/aerospace9050279

Kriebel, A. R., & Mendenhall, M. R. (1964). *Predicted and measured performance of two full-scale ducted propellers*. National Aeronautics and Space Administration.

Liu, T. (2021). Evolutionary understanding of airfoil lift. *Advances in Aerodynamics*, *3*(1), Article 37. https://doi.org/10.1186/s42774-021-00089-4

Masashi, H. (2022). Theoretical background and user's manual of ducted fan optimal design program, OptDuct. *JAXA Research and Development Memorandum*, *1*, Article 49. https://doi.org/10.20637/00048250

Moeckel, W. E. (1963). Electric propulsion. *Science*, *142*(3589), 172–178. https://doi.org/10.1126/science.142.3589.172

Muehlebach, M., & D'Andrea, R. (2017). The flying platform – a testbed for ducted fan actuation and control design. *Mechatronics*, *42*, 52–68. https://doi.org/10.1016/j.mechatronics.2017.01.001

Nugroho, G., Bramantya, M. A., Ghani, M. A., Wang, S. S., & Kurniawan, Y. A. (2018). Design, manufacture and flight test of an Electric Ducted Fan (EDF) powered cruise missile. *Journal of Physics: Conference Series*, *1130*(1), Article 012030. https://doi.org/10.1088/1742-6596/1130/1/012030

Panigrahi, D. C., & Mishra, D. P. (2014). CFD simulations for the selection of an appropriate blade profile for improving energy efficiency in axial flow mine ventilation fans. *Journal of Sustainable Mining*, *13*(1), 15–21. https://doi.org/10.7424/jsm140104

Pope, A. (1951). *Basic wing and airfoil theory* (1st ed.). the McGraw-Hill Book Company, Inc.

Ryu, M., Cho, L., & Cho, J. (2017). The effect of tip clearance on performance of a counterrotating ducted fan in a VTOL UAV. *Transactions of the Japan Society for Aeronautical and Space Sciences*, *60*(1), 1–9. https://doi.org/10.2322/tjsass.60.1

Schäfer, M. (2006). *Computational engineering – introduction to numerical methods*. Springer International Publishing. https://doi.org/10.1007/978-3-030-76027-4

Seitz, A. (2012). *Advanced methods for propulsion system integration in aircraft conceptual design* [Dissertation, Universitat Munchen]. http://mediatum.ub.tum.de/node?id=1079430

Selig, M. S. (2003). Low Reynolds number airfoil design. In *VKI Lecture Series (Low Reynolds Number Aerodynamics on Aircraft Including Applications in Emerging UAV Technology, November)*. https://m-selig.ae.illinois.edu/pubs/Selig-2003-VKI-LRN-Airfoil-Design-Lecture-Series.pdf

Sharman, R. A. (2011). Electric ducted fan – theory and practice. *RCME & Home of Model Flying*.

SolidWorks. (n.d.). *The solution for 3D CAD, design and product development*. https://www.solidworks.com/

Stosiak, M., Zawislak, M., & Nishta, B. (2018). Studies of resistances of natural liquid flow in helical and curved pipes. *Polish Maritime Research*, *25*(3), 123–130. https://doi.org/10.2478/pomr-2018-0103

Toguchi, T., Tanigawa, R., & Mizobata, K. (2016). *Design and manufacture of a scaled-down small supersonic flight experimental aircraft and preliminary flight tests*. Muroran Institute of Technology Aerospace Plane Research Center. http://hdl.handle.net/10258/00009117

Urban, D., Kusmirek, S., Socha, V., Hanakova, L., & Hylmar, K. (2023). Effect of electric ducted fans structural arrangement on their performance characteristics. *Applied Sciences*, *13*(5), Article 2787. https://doi.org/10.3390/app13052787

van Rooij, N. E. (2019). *Analysis of a 3D printed electric ducted fan for high-speed flight*. Eindhoven University of Technology.

Versteeg, H. K., & Malalasekera, W. (2007). *An introduction to computational fluid dynamics* (2nd ed.). Pearson Education Limited.

Voogd, A. E. (2020). *Experimental investigation of boundary layer ingestion in integrated propulsion systems*. Delft University of Technology.

Weintraub, D., Koppelberg, J., Köhler, J., & Jeschke, P. (2022). Ducted fans for hybrid electric propulsion of small aircraft. *CEAS Aeronautical Journal*, *13*(2), 471–485. https://doi.org/10.1007/s13272-022-00573-7

Weintraub, D. P. (2024). *Mantelpropellerantriebe für Kleinflugzeuge* [Ducted propeller drives for small aircraft]. Rheinisch-Westfälischen Technischen Hochschule Aachen.

Zhang, B., Song, Z., Zhao, F., & Liu, C. (2022). Overview of propulsion systems for unmanned aerial vehicles. *Energies*, *15*(2), Article 455. https://doi.org/10.3390/en15020455

Zhang, T. (2022). *Numerical investigation of ducted propellers for novel rotorcraft configurations* [PhD thesis, University of Glasgow].

Zhang, T., & Barakos, G. N. (2020). Review on ducted fans for compound rotorcraft. *The Aeronautical Journal*, *124*(1277), 941–974. https://doi.org/10.1017/aer.2019.164